STLE
Dallas ★ May 17-21, 2015

EXPERIMENTAL ASSESSMENT OF DRAG AND ROTORDYNAMIC RESPONSE FOR A POROUS TYPE GAS BEARING

CATEGORY Fluid Film Bearings

AUTHORS AND INSTITUTIONS
LUIS SAN ANDRÉS, Mast-Childs Chair Professor and Fellow STLE
SUNG-HWA JEUNG and MICHAEL ROHMER, Graduate Research Assistants
Mechanical Engineering Department, Texas A&M University, College Station, TX 77843, USA
ANDREW DEVITT, Chairman and Chief Technical Officer, New Way Air Bearings, Aston, PA 19014, USA

INTRODUCTION

Gas film bearings are attractive means to support rotating equipment while dispensing of complicated lubrication systems. In particular, tilting pad journal bearings with external pressurization permit operation with minute clearances and offer high stiffness for accurate positioning while operating with little shear drag and provide enhanced stability due to the absence of cross-coupled stiffnesses induced by hydrodynamic effects [1].

The paper presents measurements to evaluate the performance, static and dynamic, of novel porous carbon-graphite tilting pad gas bearings engineered for high speed applications. The bearing pads are flexibly supported, and a mechanism allows its installation with a desired clearance or specific preload. Upon supply of an external pressurized gas media, the pads push their pivots and retract towards the elastic support thus enabling friction free operation.

Porous type gas bearings differ from other hydrostatic bearing configurations that make use of orifices or grooves because sub-micron sized holes distributed in their matrix material, like a sponge, allow for an even distribution of gas flow over the entire surface of the bearing [2]. When compared to orifice restricted hydrostatic gas bearings, porous type gas bearings have higher stiffness and damping coefficients, thus finding a niche in applications demanding of high stiffness to accurately control rotor displacements induced by dynamic forces [3]. Due to challenges in manufacturing and ensuring the consistency of parts, only recently porous bearings with a carbon-graphite matrix [2] have become commercially available at a low cost. As a result, limited information is available on the physical implementation of these bearings into rotor-bearing systems operating at high surface speeds [2].

TEST RIG DESCRIPTION

Figure 1 shows photographs of the air bearing test rig and its instrumentation. In brief, two identical air bearings support a rigid rotor-motor, 0.89 kg in weight (W) and outer diameter $D=2R=28.5$ mm, as shown in the inset in Fig. 1(b). The rotor comprises of a steel shaft, 15 mm in diameter and 190 mm in length (l), onto which a two-pole motor insert and two sleeves are press-fit, see inset in Fig. 1(c). A thick hard chrome coating, thickness 0.25 mm, covers the rotor at the bearing locations. The bearings' span is 120 mm. A stiff structure holds the motor stator and the bearing supports on the sides. Two end caps with flexible thrust pins control the axial displacement of the rotor while in operation. A high frequency converter/control unit (840 W max) powers an asynchronous three-phase motor armature that drives the rotor up to 55 krpm (surface speed=82 m/s). The test rig has been used for evaluation of various types of radial gas bearings, including flexure pivot tilting pad bearings; see Ref. [4] for example with shaft speeds to 100 krpm.

Two pairs of eddy current sensors, orthogonally positioned in the support structure and facing the rotor ends, measure the rotor displacements along the vertical and horizontal planes. Oscilloscopes display the rotor orbits and a two channel analyzer shows the frequency content of the rotor displacements. A high-speed infrared tachometer sensor, mounted on a side cap and facing directly one end of the rotor, records the shaft speed and provides a keyphasor signal for data acquisition and processing. Reference [4] further details the test rig components and instrumentation.

Figure 2(a) portrays a side view of the test rig with its end cap removed to better visualize the disposition of the gas bearing; Fig. 2(b) depicts a schematic view of the three-pad porous gas bearing and its support structure, and Fig. 2(c) displays a cross-section of the pads showcasing the inlet for the air supply and the ball-type pivot with adjustment for radial preload on the rotor. Fig. 2(d) depicts a conformed bearing pad, made of porous carbon-graphite; 30.1 mm in length (L) and width, and 82.5° in arc length. The air supply line into the bearings contains a flow valve, an air filter, a pressure

regulator, a Bourdon type pressure gauge, and a flow meter to monitor and regulate the air supply. Plastic hoses, 3 mm diameter, deliver the pressurized air into each porous pad.

When installed and not yet pressurized, the porous pads and rotor have a radial clearance c=36 μm (±2 μm). This clearance can be easily adjusted, even zeroed, with the adjustment mechanism shown in Fig. 2(c).

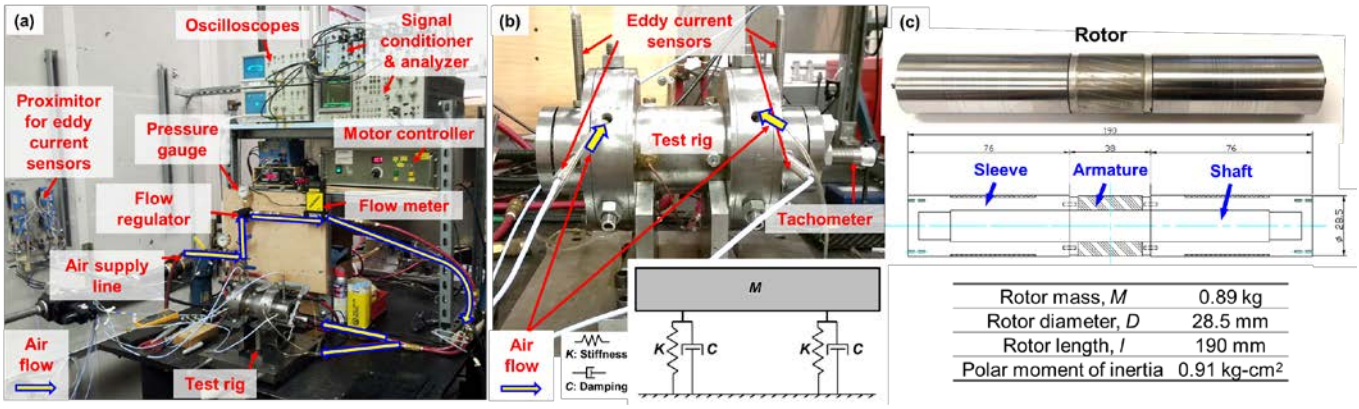

Fig. 1 Photographs of (a) gas bearing test rig and instrumentation, (b) front view of test rig with inset depicting rotor supported on its bearings, and (c) rotor-motor and main physical parameters.

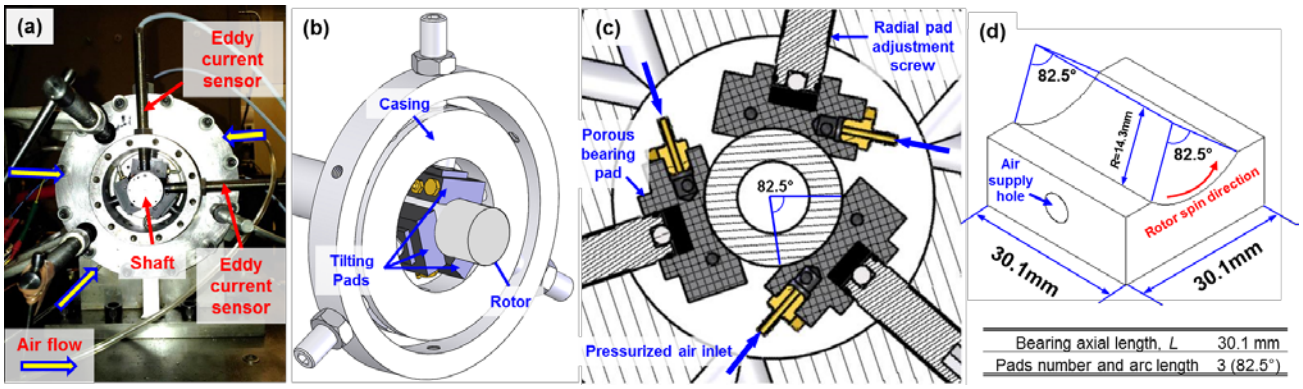

Fig. 2 (a) Photograph of side view of test rig depicting an installed gas bearing, (b) isometric view of three-pad bearing supporting rotor, (c) cross section of three-pad porous bearing and air supply, and (d) dimensions of a bearing pad.

COAST DOWN SPEED TESTS: DETERMINATION OF BEARINGS' DRAG COEFFICIENT C_Θ

The air supply line delivers pressurized gas flow to the bearings' pads and the rotor lifts offering little resistance to rotation. The minimum pressure for rotor lift off is $P_{S\text{-}min}$=3.8 bar (abs). Next, the HF driver powers the motor, and the motor spins the rotor from rest to a maximum speed of ω_0=55 krpm (916 Hz, 82 m/s surface speed). At this speed, the HF converter is turned off and the rotor coasts down to rest from its maximum speed.

Fig. 3 shows the rotor speed fraction (ω/ω_0) versus time for tests conducted with supply pressure (P_S) at 5.1, 6.5, and 7.9 bar (absolute) [60, 80, 100 psig] and air supplied at ambient temperature (~27 ºC=80 ºF). Note that an increase in supply pressure keeps the rotor spinning for a longer time. During the first instants of coast down, t < 40 s, the rotor speed –shown in logarithmic scale- decays quickly mainly due to air windage from the rotor surface; the speed reduction appears not to be affected by the air supply pressure magnitude. As the speed decreases further and below ω/ω_0 ~ 0.3, the coast down reveals (in the log scale) a linear drop in speed vs. time, i.e., an exponential type decay typical of viscous drag from the bearings. Below (ω/ω_0) < 0.1 and 0.02 for P_S=5.1 bar and 7.9 bar (abs), respectively, the rotor decelerates rather rapidly as it contacts the bearing pads, a rub condition. The labels for the curves in Fig. 3 also show the air flow rate, in liters per minute, supplied to the two bearings.

Based on the rationale above, during a coast down event, the governing equation for the rotor angular motion ($\omega_{(t)}$) is

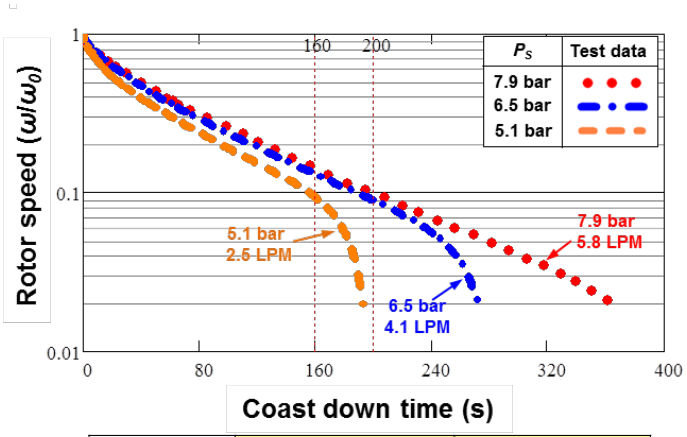

Supply pressure (bar)	Bearing drag coefficient, C_θ (N.μm.s/rad)	Friction coefficient, μ_f @ 10 krpm
7.9	0.25	0.004
6.5	0.30	0.005
5.1	0.43	0.007

Fig. 3 Recorded rotor speed fraction (ω/ω_0) vs. time during coast down test from ω_0=55 krpm. Air supply pressure P_S = 5.1, 6.5, 7.9 bar (abs). Table shows identified bearing drag coefficient C_θ vs. supply pressure.

$$I_P \frac{d\omega}{dt} + T_{drag} = I_P \frac{d\omega}{dt} + 2T_{bearing} + T_{windage} = 0 \qquad (1)$$

where I_P =0.91 kg-cm^2 is the rotor polar mass moment of inertia. The drag torque accounts for the shear torque from both bearings (2 x$T_{bearing}$) and the torque from rotor windage losses ($T_{windage}$). For the bearings, the drag is assumed of viscous type,

$$T_{bearing} = C_\theta \omega \qquad (2)$$

with C_θ as a rotational drag coefficient. Windage losses occur over the rotor surface not exposed to the bearings, its area being ~ πD^2 (l-2L), with l as the rotor length and L as a bearing length. The drag torque from windage is [5]

$$T_{windage} = \tfrac{1}{4} C_D \rho \left(\tfrac{1}{2}\omega D\right)^2 \left[\pi D^2 (l - 2L)\right] \qquad (3)$$

where C_D, a coefficient of windage loss, is a function of the Reynolds number, Re = $\tfrac{1}{2}(\rho/\mu)\omega D c_t$, with c_t=1mm as the air gap between the rotor and is armature.

For turbulent flow conditions [5] ,

$$1/\sqrt{C_D} = 2.04 + 1.768 \ln\left(\sqrt{\mathrm{Re}}\right) \qquad (4)$$

Note that at ω_0=55 krpm, Re=5,400 well into the turbulent flow regime, *Re* >> 400 [6]. A numerical method solves Eqs. (1-4) and delivers the rotational drag coefficient C_θ for one bearing and valid for operation with speed $\omega > 0.1\omega_0$. The inset in Fig. 3 lists C_θ, decreasing as the gas supply pressure magnitude increases. From C_θ, a friction factor μ_f = $T_{bearing}/(W\ R)$, with W as ½ the rotor weight, also follows. Fig. 3 also lists at ω/ω_0 =10/55, a friction factor (μ_f) that decreases as the magnitude of gas supply pressure increases. For P_S=7.9 bar and 5.1 bar (abs), the solution of Eq. (1) gives $T_{windage}/(2T_{bearing})$=2.5 and 1.5 at the top speed ω=55 krpm, whereas $T_{windage}/(2T_{bearing})$= 0.4 and 0.2 at 5.5 krpm (ω/ω_0=0.1), respectively. As expected, the model shows windage losses is the dominant drag source at high rotor speed.

ROTORDYNAMIC RESPONSE DURING ROTOR ACCELERATION AND COAST DOWN

A data acquisition system records the rotor speed and the shaft displacement (vertical and horizontal) at the ends of the rotor as it accelerates in speed to ω_0; and then with the motor unpowered, coasts down to rest. Fig. 4 displays the synchronous amplitude of rotor displacement as it crosses the first (rigid body) critical speed. The response shown is due to the rotor remnant imbalance, with slow roll compensation at 1 krpm, and for operation at three magnitudes of supply pressure (P_S). External pressurization has a small effect on the natural frequency but a significant one on the system damping ratio. The table in Fig. 4 shows the rotor-bearing system has a damping ratio (ζ) that decreases from 17.2% to 11.0% as P_S increases from 5.1 bar to 7.9 bar. The system natural frequency (first critical speed) changes little with gas pressure (P_S) into the bearings; that is, 8.9 krpm (148 Hz) at P_S =5.1 bar (abs) and 8.1 krpm (135 Hz) at P_S =7.9 bar (abs).

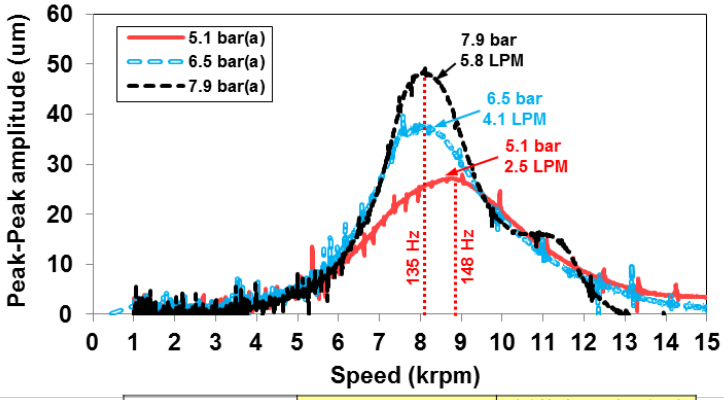

Supply pressure (bar)	Damping ratio, ζ	1st Undamped natural frequency, (Hz)
7.9	0.110	135
6.5	0.140	136
5.1	0.172	148

Fig. 4 Peak-peak amplitude of rotor synchronous response versus shaft speed. Displacements at rotor left end, vertical plane (LV). Air supply pressure P_S = 5.1, 6.5, 7.9 bar (abs). Response due to remnant imbalance in rotor.

Fig. 5 shows waterfall (top) and cascade (bottom) plots of the amplitude of rotor motion as the rotor ramps up to 55 krpm and then coasts down. From left to right, the air supply pressure into the bearings equals P_S=7.9, 6.5, and 5.1 bar (abs). On each waterfall in Fig. 5 (top), the horizontal axis depicts the frequency content of the rotor motion and the vertical axis displays the time of measurement. On each cascade plot in Fig. 5 (bottom), the horizontal axis represents frequency and the vertical axis displays the shaft speed. The rotor response, recorded at the rotor left end, is mainly synchronous (1X). On each graph, an oval encloses a region of incipient subsynchronous whirl, varying in onset speed and amplitude, albeit locked at the first natural frequency. As P_S decreases, the rotor motions at the system natural frequency begin at a lower shaft speed and its intensity (amplitude) seems to increase. Note, however, the rotor-bearing system does not display a self-excited whirl instability, i.e., subsynchronous whirl motions of growing amplitude.

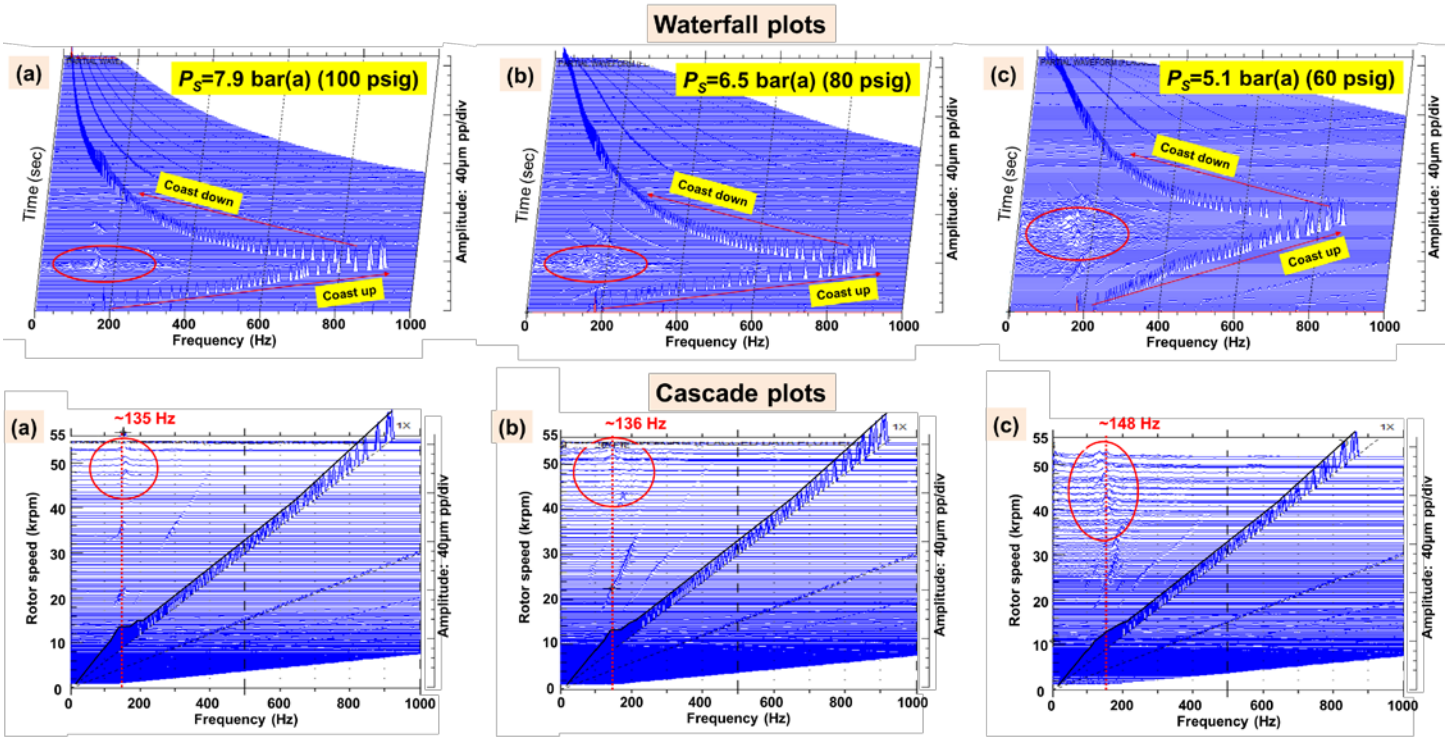

Fig. 5 (top) Waterfall plots of amplitude of rotor motion during acceleration to 55 krpm and coast down to rest; (bottom) cascade plots during acceleration to 55 krpm. Operation with bearings supplied with air at (a) 7.9 bar (abs), (b) 6.5 bar (abs), and (c) 5.1 bar (abs). Displacements measured at the rotor left end, vertical direction (LV).

CONCLUSION

The extended abstract details the operation of a rigid rotor supported on three-pad carbon-graphite (porous) bearings supplied with pressurized air at 5.1, 6.5, and 7.9 bar (abs). Measurements of the rotor speed during a coast-down show the bearings operate with viscous drag, indicative of an established thin film that is a function of the magnitude of external pressurization. The higher the supply pressure, the lower the drag and the longer the time for near friction-free operation. Rotor lateral motions to a top speed of 55 krpm reveal a well behaved system with mainly synchronous frequency amplitude displacement. The rotor crosses a rigid-body mode critical speed at ~ 8.9 krpm (148 Hz) for P_S =5.1 bar (abs) and ~ 8.1 krpm (135 Hz) for P_S =7.9 bar (abs). An increase in the supply pressure to the bearings determines a significant drop in damping ratio (ζ) from 17.2% to 11.0%. Rotor motions at speeds well above its critical speed reveal the onset of incipient subsynchronous whirl motions, slightly more severe as the supply pressure into the bearings decreases. The noted whirl motions are rather benign, i.e. not a precursor to a rotordynamic instability.

Future work will investigate the effect of mechanical preload on the drag torque and the identification of rotordynamic force coefficients for this type of porous gas bearing. Presently, the limited experimental validation demonstrates the novel gas bearings are reliable supports though needing of an external pressurization source to enable their near friction-free operation.

ACKNOWLEDGMENTS
Thanks to New Way Air Bearings (http://www.newwayairbearings.com) for donating the test bearings and preparing the 3D drawings.

REFERENCES
[1] San Andrés, L., 2010, *Modern Lubrication Theory* "Gas Film Lubrication," Notes 15, Texas A&M University Digital Libraries, https://repository.tamu.edu/handle/1969.1/93197
[2] Devitt, A., 1999, "Porous vs. Orifice Air Bearing Technology," Technical Report, New Way Bearings, http://www.newwayairbearings.com/sites/default/files/new_way_white_papers_history_of_air_bearings_1999-04.pdf
[3] Sneck, H., 1968, "A Survey of Gas-Lubricated Porous Bearings," Tribology International, pp. 804-809.
[4] San Andrés, L., and Ryu, K., 2008, "Hybrid Gas Bearings with Controlled Supply Pressure to Eliminate Rotor Vibrations while Crossing System Critical Speeds," ASME J. Eng. Gas Turbines Power, **130**, p. 062505.
[5] Vranick, J. E., 1968, "Prediction of Windage Power Loss in Alternators," NASA Report TN D-4849.
[6] Walton, J.F., Heshmat, H., and Tomaszewski, M., "Power Loss in High-Speed Micro Turbomachinery - an Experimental Study," ASME Paper GT2012-69558.

KEYWORDS
Hydrostatics: Air Bearings, Porous Bearings, Hydrostatics: Tilting-Pad Bearings.